Hindawi
Journal of Nanomaterials
Volume 2023, Article ID 5012576, 17 pages
https://doi.org/10.1155/2023/5012576

Research Article

The Biocompatibility and Antibacterial Properties of the CNTs-Doped Magnesium Based Composite Implants in a Long-Term Biodegradation Process

Meng Zhao,[1,2] **Rongjun Su**,[3] **Lingyu Ji**,[3] **Ying Zhang**,[1] **Huirong Wu**,[1] **Zhaohui Wen**,[1] **and Changsong Dai**[4]

[1]*Department of Neurology, First Affiliated Hospital of Harbin Medical University, Harbin 150001, China*
[2]*Department of Magnetic Resonance Imaging, Cangzhou Central Hospital, Cangzhou 061000, China*
[3]*Environmental Science and Engineering, Harbin University of Commerce, Harbin 150001, China*
[4]*School of Chemistry Engineering and Technology, Harbin Institute of Technology, Harbin 150001, China*

Correspondence should be addressed to Zhaohui Wen; wenzhaohui1968@163.com

Received 10 March 2022; Revised 21 November 2022; Accepted 30 November 2022; Published 22 January 2023

Academic Editor: Muhammad Wahab Amjad

The aim of this paper is to increase a new biodegradable implant material's biodegradability, biocompatibility, and osteoinductivity in the long-term degradation process, as well as its antibacterial properties, novel carbon nanotubes (CNTs) with or without Cu element were doped into calcium phosphate (CaP)–chitosan (CS) layers and then fabricated to obtain the magnesium (Mg) matrix composites. In this paper, we investigated the influences of the CNTs-CaP-CS/Mg composites on proliferation and osteogenic differentiation of human osteosarcoma cell (SaOS-2) and human bone marrow mesenchymal stem cells (*h*BMSCs). Furthermore, the Cu/CNTs-CaP-CS/Mg was prepared to improve the bioactivity and antibacterial activity of the composites. The results indicated that CNTs-CaP-CS/Mg composites were suitable for proliferation and differentiation of SaOS-2 cells. Stimulated by the CNTs-CaP-CS/Mg extracts, the ALP expression of *h*BMSCs increased in the first 16 days and the mineralization ability of *h*BMSCs was highly expressed throughout the whole process which might be through the Erk1/2 signaling pathway. After CNTs-loaded Cu element, the bioactivity of the coating was satisfactory. Moreover, this new implant exhibited excellent antibacterial properties for *Escherichia coli* (*E. coli*) and *Staphylococcus albus* (*S. albus*). Collectively, these data suggest that the CNTs-CaP-CS/Mg and Cu/CNTs-CaP-CS/Mg might be potentially applied as bone implants for future clinical use.

1. Introduction

Bone implants typically require both mechanical support and osteogenesis to set up the right environment to stimulate new bone tissue during bone healing [1]. As a new trend for the repair, regeneration, and substitution of bone defects, biodegradable magnesium (Mg) alloys have attracted much attention due to their advantageous properties [2–5]. The corrosion and degradation of Mg implants can be effectively metabolized and excreted through urine [6]. The density of Mg alloys is substantially equal to human bone mineral density [7], and the mechanical strength and elastic modulus of Mg alloys are alike cortical bone, which can reduce the stress shielding effect on the surrounding bone and avoid the second surgery [8–10]. The biodegradable Mg implants have a long history of application in biomedical field [11]. There are, however, a series of questions that still need to be resolved before widespread clinical application takes place, especially regarding the high corrosion rate [8]. Complex biological and sensitive human body system require implants with manifold characteristics. First, to match cell/tissue growth, bone implants should have a controllable degradation and bone resorption rate and to match those of the tissues at the site of implantation, its mechanical behavior needs to be sufficient. In addition, its degradation products must be nonpoisonous, maintain cell vitality, suitable for cell differentiation, and possess the ability to induce bone regeneration [12]. Currently, single-ingredient materials in mechanical strength, degradation rate, biological activity,

bone induction, and other aspects existed many problems. In recent years, many scholars have made a variety of composites, especially nanocomposites to realize the complementary advantages of the material, so that performance is greatly improved [13].

To ameliorate the degradation rate and biocompatibility of Mg and Mg alloys, ceramic coating with superior performance was widely used. Hydroxyapatite (HA), which is the main mineral composition in the hard tissue of human bones systems and can induce the formation of bone-like apatite layer in the body environment, is a bioceramic material often used for clinical bone grafting and implantation [14–16]. Chitosan (CS) has good thermal stability and mechanical strength which can make up for the inherent disadvantages of HA with low tensile strength and fracture toughness [17, 18]. Carbon nanotubes (CNTs) also have excellent mechanical properties which can further enhance the strength and toughness of fragile HA ceramic coating, it possesses higher reactivity for interactions involved in the cell attachment mechanism and can offer a favorable condition to induce cellular functions [19–21]. It has been proved that the incorporation of CNTs as an adjuvant ingredient into bioactive coating can promote the attachment, proliferation, and differentiation of osteoblast by providing the appropriate nanostructured surface of the pore walls and then lead to biodegradable nanocomposites with excellent comprehensive properties [22–24]. In our previous studies, a novel CNTs-CaP-CS magnesium matrix composites (CNTs-CaP-CS/Mg) was designed as bone substitution material. Electrochemical tests were conducted with those composites in different immersion times, and the increase in corrosion resistance was reported [25]; however, as biodegradable materials the biocompatibility of those composites was not reported, which was essential for further improvement and clinical application of bone implants.

Bacterial infection after the implantation operation is considered as one of the biggest disastrous complications and the major cause of implant failure, and thus the improvement of antibacterial property of bone implant is of great significance to prevent these bacterial infections. The antibacterial activity can be generally improved through loading metal ions [26], blending bactericides [27], modifying surface with antibacterial properties such as copper, silver, etc. [28, 29]. Copper (Cu) with the bactericidal capability which had effectively inhibitory effects on the growth of bacteria, fungi, and algae has been known for decades [30]. Moreover, Cu as an essential element for living organisms does not develop bacterial resistance and its price is relatively low in the market which would prove to be very economical [31–33]; hence, it is more suitable for biomedical application as bactericides. Previous researches have shown that Cu-containing nanocomposites possessed excellent antibacterial properties and favorable biocompatibility and its products might meet hospital requirements [34–36].

In this paper, we primarily investigate the influences of the CNTs-CaP-CS/Mg degradation products on human osteosarcoma cell line (SaOS-2) and human bone marrow mesenchymal stem cells (*h*BMSCs) during the nearly 4-month degradation process. Furthermore, the CNTs-CaP-CS coating incorporated with Cu element was prepared and its bonding strength, biological activity, and antibacterial activity were investigated.

2. Materials and Methods

2.1. Preparation of CNTs-CaP-CS/Mg Composites

2.1.1. Fabrication of CNTs-CaP-CS/Mg and Cu-CNTs-CaP-CS Coating. The microarc oxidized (MAO) process, wet chemical precipitation technology for nanohydroxyapatite (*n*HA), and electrophoresis deposition (EPD) were prepared as in the previous work [37, 38]. The aqueous solutions required for EPD were performed as described follows: 0.25 g CS, 1.0 g *n*HA, 0.2 g CNTs, and 0.05 g (or without) $Cu(NO_3)_2$ particles were sequentially added into a 200 ml aqueous solution containing 9 ml of acetic acid under stirring, respectively, and 1.5 g *n*HA particles were added to 300 ml absolute ethanol to obtain a second solution.

2.1.2. Immersion into m-SBF. After immersion in the PBS, four of each of the CNTs-CaP-CS/Mg and Cu/CNTs-CaP-CS/Mg samples were put into the m-SBF and immersed for 6, 12 hr, 1, 2, 8, 16, 24, 34, 44, 60, 90, and 120 days at 37°C, respectively [39]. The ratio of the sample surface area (cm^2) to the m-SBF volume (ml) was 1 : 250. The samples at different time points were removed from the m-SBF and the extraction solutions were prepared for further research.

2.2. In Vitro Biocompatibility Studies

2.2.1. Cell Viability Assay. The CCK assay was employed to measure the cytotoxicity of the CNTs-CaP-CS/Mg extracts to SaOS-2 (ScienCell, USA) cells during the long-term degradation process [40]. First, 5×10^3 cell/100 μl cells were cultured in McCoy's 5A medium (Sigma) on 96-well plates at 37°C in an atmosphere of 5% CO_2 and 95% air for 1 day and then those old culture mediums were replaced with 100 μl new culture medium containing 50% CNTs-CaP-CS/Mg extracts. After 3 days, the absorbance of cells cultured in different extracts at 450 nm was measured with CCK8 solution (Dojindo, Japan) in Elx-800 (Bio-Tek Instruments) and the cell viability was worked out as reported by the instructions.

2.2.2. Cytoskeleton Staining Experiments. The cytoskeleton staining was used to analyze the cell morphology after SaOS-2 cells (1×10^5 per well) cultured in 50% CNTs-CaP-CS/Mg extracts for 3 days. After being washed with PBS, the cells were fixed in a fixative solution which was synthesized by 4% paraformaldehyde for 10 min and permeabilized with 0.1% Triton X-100 for 5 min. Using the fluorescent microscope (Nikon, Japan), the samples were observed and recorded after double staining with rhodamine-phalloidin (200 μl 100 nM; Cytoskeleton, USA) and 4′,6-diamidino-2-phenylindole (DAPI) (200 μl 100 nM; Beyotime, Shanghai, China).

2.2.3. Apoptosis Detection. The Annexin V–fluorescein isothiocyanate (FITC) apoptosis detection kit (BD Biosciences, San Diego, USA) was used to measure apoptosis after SaOS-2 (3×10^5 per well) cultured in the 50% CNTs-CaP-CS/Mg extracts for 3 days. Both suspension and adherent cells

were gathered by centrifugation, washed with cold PBS, resuspended with 1 × cold binding buffer, and then stained with Annexin V and propidium iodide (PI) for 15 min. Finally, flow cytometry (BD, USA) was used to detect apoptosis, and Cell Quest software (BD, USA) was employed to evaluate the information.

2.3. In Vitro Osteogenic Differentiation Studies

2.3.1. Alkaline Phosphatase (ALP) Activity Assay. The ALP Assay Kit (Beyotime, Shanghai, China) was used to test the ALP activity of SaOS-2 cells (1×10^4 per well) which were treated with 50% CNTs-CaP-CS/Mg extracts for 3 days. After 12 hr incubation in 0.1% Triton X-100 (Sigma) at 4°C, the reaction was stopped and the ALP activity was measured and presented as nmol p-nitrophenol (PNP) manufactured per minute.

2.3.2. ALP and Alizarin Red S Staining Assay. The *h*BMSCs (ScienCell, 7500, USA) were cultured for 14 days in CNTs-CaP-CS/Mg mixed mediums which were replaced every 2 days and then fixed with 4% paraformaldehyde. The obtained cells were stained with BCIP/NBT ALP kit (Beyotime, Shanghai, China) and 2% Alizarin Red S Stain Solution (ScienCell, USA), respectively [40]. The colorimetric endpoint assay was used to determine the quantitative ALP activity, and after eluted by cetylpyridinium chloride at 590 nm the quantitative estimation of calcium deposition was assayed.

2.3.3. Western Blot Analysis and Pathway Inhibition. The *h*BMSCs were incubated with m-SBF, several selected CNTs-CaP-CS/Mg extracts and CaP-CS/Mg extracts for 3 days and cell proteins were extracted as previously described [40]. Briefly, the total proteins were extracted and separated by SDS lysis buffer (Beyotime, Shanghai, China) containing 1 mM phenylmethylsulphonyl fluoride (PMSF, Beyotime, China) and subsequently transferred onto polyvinylidene fluoride (PVDF) membranes. The PVDF membrane was incubated overnight at 4°C with p-Erk2/1, total-Erk2/1 (1 : 2,000, rabbit monoclonal antibodies, CST, USA), phospho-Akt (p-Akt), total-Akt (1 : 1,000, rabbit monoclonal antibodies, CST, USA), and β-actin (1 : 1,000, mouse monoclonal antibodies, CST, USA) and incubated with secondary antibodies for 1 hr. The PD98059 (Erk2/1 inhibitor, CST, USA) was used to inhibit the pathway. To observe the influence of pathway inhibition on the cell osteogenic differentiation more directly, the ALP assay and Alizarin Red-S assay were examined after *h*BMSCs were treated with 2 and 60 days extracts containing inhibitors for 14 days, respectively.

2.4. Specimen Characterization. The strength comparison of CNTs-CaP-CS/Mg and Cu/CNTs-CaP-CS/Mg was tested by scarification condition. The element concentrations and the pH values in the sample extracts at different time intervals (0, 3, 7, 14, 21, and 28 days) were detected. The X-ray diffractometer (XRD, Rigaku D/max-γB), Fourier-transformed infrared spectrophotometer (FTIR, AVATAR360, Nicolet Instruments), Raman spectrometer (DXR, Thermo Scientific), and a thermogravimetric (TG) analyzer and a differential thermal analyzer (DTA, ZRY-2p, Shanghai Precision & Scientific Instrument Co., China) were adopted to analyze deposit composition [38].

2.5. Antibacterial Activity Assay. The antibacterial activity of the CNTs-CaP-CS and Cu/CNTs-CaP-CS coatings was tested against Gram-negative bacteria (*Escherichia coli* (*E. coli*)) and Gram-positive bacteria (*Staphylococcus albus* (*S. albus*)). The coatings after disinfection were placed in the same agar medium inoculated with *E. coli* and *S. albu*s, and incubated at 37°C for 24 hr. After measured the size of the bacterial inhibition ring, the coatings were put into the new medium *E. coli* and *S. albus*, and then the bacterial inhibition rings were measured and the mediums were replaced every 3 days. The size and duration of the two groups were recorded.

The *E. coli* and *S. albus* were added to the surface of the coatings evenly and incubated at 37°C for 24 hr. Then the bacteria in the coatings were eluted with 1.9 ml PBS solution on the vortex oscillator for 5 min. Each of the 100 μl elution liquid was pushed into the flat plate and the colony-forming unit was counted after incubation at 37°C for 3 days.

2.6. Statistics. All statistics are displayed as the means ± standard deviations from three independent experiments. The comparison of different groups was analyzed using a one-way analysis of variance (ANOVA) and the Tukey test. $P < 0.05$ was considered statistically significant.

3. Results and Discussion

The preparation and characteristics of CNTs-CaP-CS/Mg were investigated in our previous study [25]; however, how their degradation products affect cell proliferation and differentiation at each specific time is crucial for further debugging and application of materials. Meanwhile, the improvement of the antibacterial activity of composites is essential to prevent postoperative complications and ensure the success of the operation.

3.1. Effects of CNTs-CaP-CS/Mg Extracts on SaOS-2 Cells

3.1.1. Proliferation of SaOS-2 Cultured in CNTs-CaP-CS/Mg Extracts. Figure 1 shows the cell viability of SaOS-2 cultured in the CNTs-CaP-CS/Mg and CaP-CS/Mg extracts. In the 6 hr extract, the two groups showed similar cell viability, and the cell viability of the CNTs-CaP-CS/Mg group was slightly higher than that of the CaP-CS/Mg group at all the other time points. The osteoblasts cultured in CNTs-CaP-CS/Mg extracts performed good tolerability with the cell viability ranging from 116.8% to 82.6% until 90 days. Before 90 days, there were no significant differences among groups. The cell viability only gradually increased when immersion time changed from 6 hr to 24 days and then decreased slightly from 34 to 90 days. It could be informed that our CNTs-CaP-CS/Mg composites could maintain excellent biocompatibility for at least 90 days, and the 24 days extract was the best. Our previous studies showed that Mg concentration was prolonged with the prolongation of immersion time [25], and the Mg concentration profile during this test was about the range between 0 and 800 ppm. When the immersion time was prolonged to 120 days, a significantly cytotoxic effect appeared and the

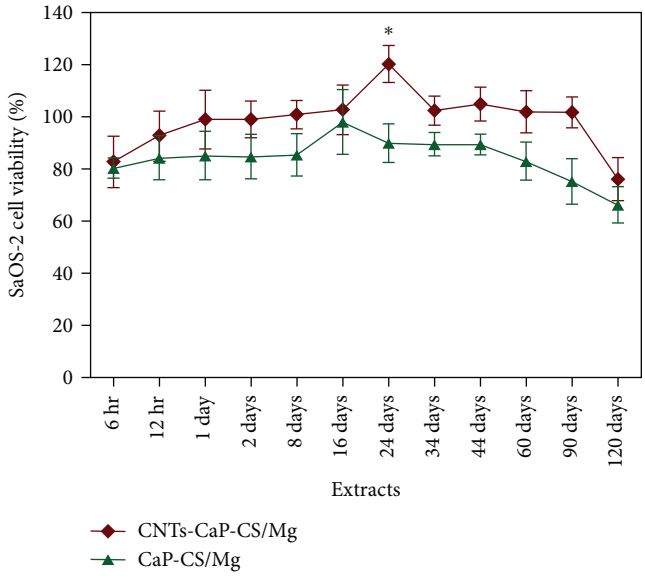

Figure 1: The cell viability of SaOS-2 cultured in 50% CNTs-CaP-CS/Mg and CaP-CS/Mg extracts (6, 12 hr, 1, 2, 8, 16, 24, 34, 44, 60, 90, and 120 days). Cells cultured in McCoy's 5A medium containing 50% m-SBF were set as control. $^*P<0.05$ compared with the control group.

cell viability was only 62.2%. Similar research had shown that the cell viability was significantly reduced when the Mg concentration was greater than 500 ppm [41]. Thus, we speculated that one of the reasons for the obvious cytotoxicity in 120 days might be the high Mg concentration.

3.1.2. Cell Morphology and Apoptosis Analysis of SaOS-2 Cultured in CNTs-CaP-CS/Mg Extracts. After cultured with different CNTs-CaP-CS/Mg extracts, the immunofluorescence staining method was used. As shown in Figure 2, the cells cultured in 6 and 12 hr extracts manifested as evenly stained cells with well-stretched actin stress fibers. The appearance of the cells cultured with 1–8 days extracts exhibited a slight difference compared with 6 hr, with the extensibility of stress fibers slightly reduced. When immersion time increased from 16 to 90 days, partial cells exhibited spindle-like shapes and cells increasingly appeared damaged and necrosis. It was observed that SaOS-2 cells in the 120 days extract exhibited an irregular shape, their stress fibers were not as well stretched as in the other groups, and their number decreased significantly compared with the 6 hr extract group. The nuclei of each group were clearly visible and had good morphology.

Annexin V-FITC and PI staining on SaOS-2 cells by flow cytometry were used to analyze the cytotoxicity of the extracts on SaOS-2 cells, and to observe the effect of different extracts on the apoptosis of SaOS-2 cells after 3 days of culture. Annexin V-FITC-stained cells without PI were considered as early apoptotic, while only PI-stained cells were considered as necrotic. Both Annexin V-FITC and PI staining showed late apoptosis. As shown in Figure 3, there is almost no cytotoxic effect when SaOS-2 cultured in the 6 hr to 90 days CNTs-CaP-CS/Mg extracts, the viable cell rate changed from 82.5% to 87.4% and the early apoptosis rate ranged from 5.2% to 11.5%. Similar studies showed that rapid corrosion of Mg alloy would cause obvious alkaline environment and exorbitant Mg concentration and it might promote cell apoptotic [42]. The 120 days extract resulted in a greater degree of apoptotic cell death and its viable cell rate was about 55.8% and early apoptosis rate was 29.8%. Our results indicated that the Mg concentration could be maintained at an appropriate concentration from 6 hr to 90 days, which is advantageous to cell proliferation.

3.1.3. Osteogenic Differentiation of SaOS-2 Cultured in CNTs-CaP-CS/Mg Extracts. To analyze the influence of CNTs-CaP-CS/Mg extracts on the differentiation of SaOS-2, we conducted ALP activity which is an early marker of early differentiation. Those factors that affect ALP expression may further affect the osteogenic mineralization ability of the cell. Figure 4 indicates that the ALP activity of SaOS-2 cells cultured in the 50% CNTs-CaP-CS/Mg extracts for 3 days. It can be seen that SaOS-2 cultured in all CNTs-CaP-CS/Mg experimental groups displayed significantly higher ALP activity than the control ($P<0.05$). Our previous experiments showed that during the entire immersion time the concentrations of Ca and P elements in the extracts roughly decreased, while Mg concentration and pH values increased [25]. It could be seen that the ALP activity of SaOS-2 reduced when immersion time increased from 6 hr to 2 days, which indicated that the decreased ALP activity might be due to the reduction of Ca and P elements. An elevated concentration of calcium and phosphate is crucial for in vitro osteogenic differentiation and cell mineralization [43, 44]. With the gradual release of degradation products especially CNTs, an increasing trend appeared and a peak followed at 24 days and then decreased. Furthermore, another increase was observed from 34 to 60 days and then decreased again, which might be related to the increased concentration of Mg. In the long-term degradation process, the promoting effect of CNTs-CaP-CS/Mg composites on osteogenic differentiation could be maintained for at least 90 days, in which the 24 days extract possessed the strongest osteoinductive.

3.2. Effects of CNTs-CaP-CS/Mg Extracts on hBMSCs

3.2.1. Osteogenic Differentiation of h*BMSCs Cultured in CNTs-CaP-CS/Mg Extracts.* In order to further explore and visually demonstrate the osteogenic differentiation of CNTs-CaP-CS/Mg, ALP staining was performed on *h*BMSCs after being treated with different extracts for 14 days. As shown in Figure 5, the degree of ALP staining gradually deepened from 6 hr to 2 days, peaked at 2 days, and then gradually decreased with time, the staining degree of ALP in the 6, 12 hr, 1, 2, 8, and 16 days groups were substantially higher than that in the control group, and the difference has statistical significance ($P<0.05$). Calcium deposition analysis was performed by Alizarin Red S staining to evaluate the influence of CNTs-CaP-CS/Mg on cell mineralization during the whole degradation process. As shown in Figure 6, the staining degree of all experimental groups was higher than that of the control group, the formation of calcium nodules could be

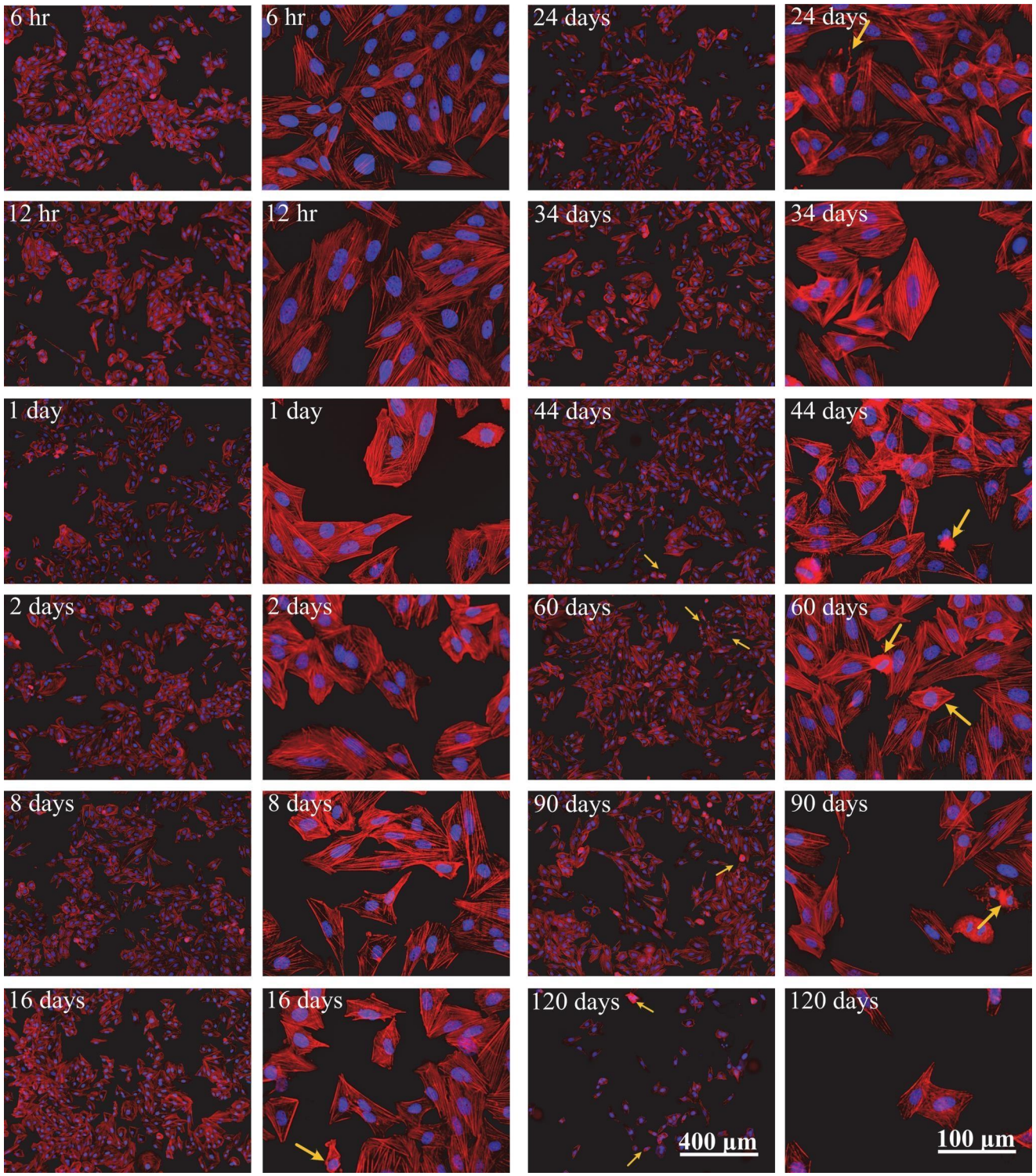

Figure 2: SaOS-2 cell morphology and fluorescence staining of F-action and nuclei after incubation with 50% CNTs-CaP-CS/Mg extracts for 3 days.

shown at 16, 24, and 60 days, and the strongest dyeing group was 60 days. Most of the research materials facilitate the osteogenic differentiation of stem cells based on the stimulation of osteogenic inducers, so the staining expression of ALP and calcium deposition is more obvious than in this study [45, 46]. Despite this, our materials showed a good ability to promote osteogenic differentiation without osteogenic supplements. Stimulated by the CNTs-CaP-CS/Mg extracts, the ALP expression of *h*BMSCs increased in the first 16 days, which is also a critical period of bone fiber growth, and the

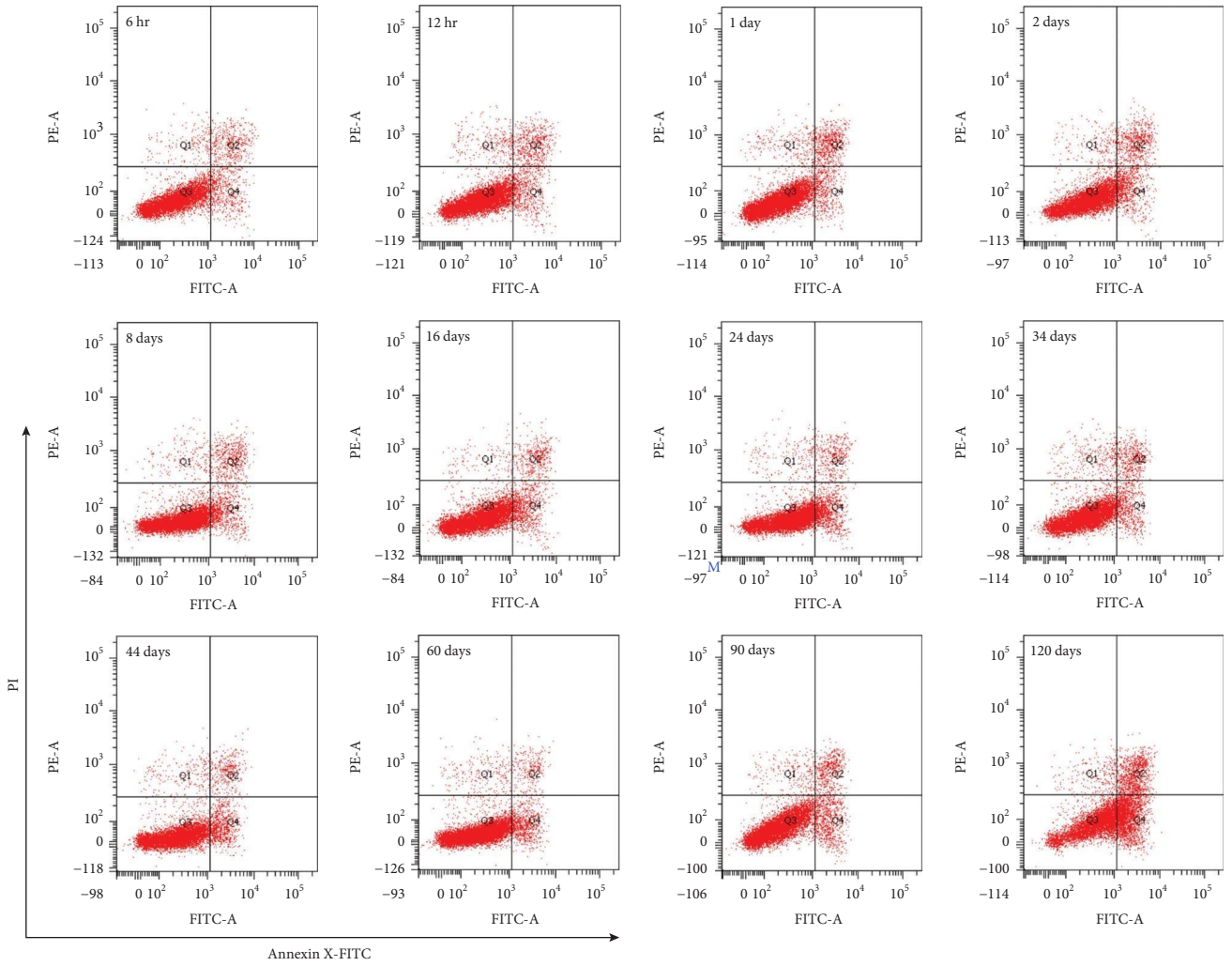

(a)

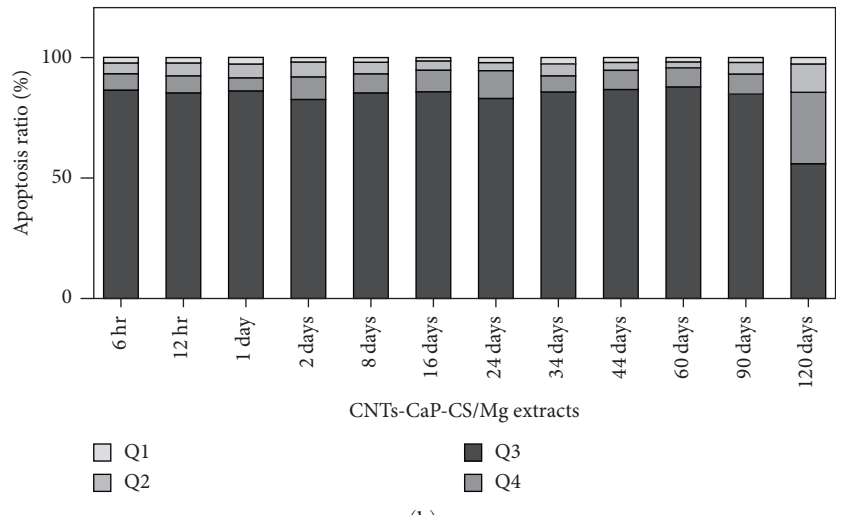

(b)

Figure 3: Flow cytometric analysis of SaOS-2 cells stained with Annexin V-FITC and PI after incubation with 50% CNTs-CaP-CS/Mg extracts for 3 days: (a) unchanged viable cells located in Q3, early apoptotic cells in Q4 (Annexin V-FITC positive), nonviable or late apoptotic/necrotic cells in Q2 (Annexin V-FITC/PI double positive) and nonviable necrotic cells/nuclear fragments in Q1 (PI single positive); (b) corresponding ratio of apoptosis in different CNTs-CaP-CS/Mg extracts.

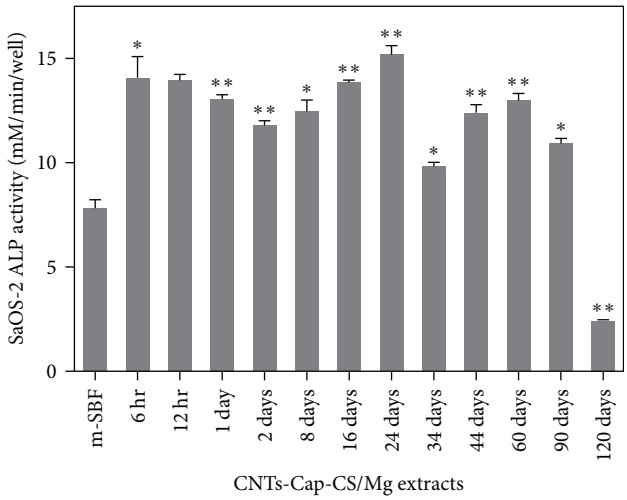

Figure 4: The ALP activity of SaOS-2 cells cultured in 50% GNS-CaP-CS/Mg extracts (6, 12 hr, 1, 2, 8, 16, 24, 34, 44, 60, 90, and 120 days) expressed as nmol ml^{-1} PNP produced per min per well. Cells cultured in McCoy's 5A medium containing 50% m-SBF were set as the control group. $^{*}P<0.05$ compared with the control group. $^{**}P<0.01$ compared with the control group.

mineralization ability of *h*BMSCs is highly expressed throughout the process.

3.2.2. Effects of Erk/MAPK Pathway Activation by CNTs-CaP-CS/Mg Extracts. Except for the osteoinductive effect, we also preliminarily explored the molecular mechanism of CNTs-CaP-CS/Mg nanocomposites promoting osteogenic differentiation of *h*BMSCs. Western blot analyses revealed that CNTs-CaP-CS/Mg extracts (12 hr, 2, 16, 34, and 60 days) facilitated the phosphorylation of Erk1/2 (Figure 7(a1)). Furthermore, we compared the expression of p-Erk in extracts of two composites (Figure 7(b)), the effects of CaP-CS/Mg 12 hr and 2 days groups were higher than those of CNTs-CaP-CS/Mg and the effects of CaP-CS/Mg 16 and 34 days groups were lower than those of CNTs-CaP-CS/Mg, while, the expression of p-Erk in 34 days of CaP-CS/Mg was low, even slightly lower than that in the control group. We suspected that the reason for this phenomenon might be due to the early degradation of the CaP-CS/Mg composites was fast. The generated calcium might be beneficial to the expression of p-Erk within an appropriate range, while the increased magnesium and pH values might inhibit the expression of p-Erk along with further degradation. The CNTs-CaP-CS/Mg nanocomposites showed a greater and longer osteogenesis effect than the CaP-CS/Mg, which further proved that the addition of CNTs might improve the corrosion resistance and osteoinductivity of materials. In this research, we also used Erk1/2-specific inhibitor PD98059 to verify whether CNTs-CaP-CS/Mg-activated p-Erk and the subsequent upregulation of ALP activity and osteogenic mineralization via the Erk1/2 signaling pathway (Figures 7(c) and 8). As shown in Figure 7(c), the expression of p-Erk induced by CaP-CS/Mg and CNTs-CaP-CS/Mg 16 days was significantly depressed in the presence of PD98059. The ALP activity and the extracellular calcium deposition of the *h*BMSCs after cultured with 2 and 60 days extracts were significantly inhibited after the inhibition of Erk1/2 phosphorylation. The above results further supported our hypothesis that CNTs-CaP-CS/Mg promoted the osteogenic differentiation and mineralization of stem cells via the Erk1/2 signaling pathway.

Both CNTs and CaP could enhance the osteogenic differentiation of osteoblast and BMSC and their combinations might be good substrates for bone regeneration. In almost the whole degradation process, our CNTs-CaP-CS/Mg composites demonstrated good biological behaviors of BMSCs in vitro, including cell morphology, apoptosis analysis, proliferation, and osteogenic differentiation. Cell morphology and viability played important roles in the expression of cell functions [47]. During the 120-day degradation process, which was also the critical period of bone growth, the cells cultured in CNTs-CaP-CS/Mg extracts were elongated and slender shaped and connected to the neighboring cells by filopodia and their viability was almost unaffected, which was beneficial to the expression of the cell phenotype. As we know, Ca plays an important role in the expression of osteogenic differentiation and could stimulate the Erk pathway [40]. Compared with CaP-CS/Mg, the 2 days and later CNTs-CaP-CS/Mg extracts were demonstrated to enhance the expression of Erk1/2 signaling pathway of BMSCs. Moreover, the CNTs-CaP-CS/Mg extracts showed good promotion of cell differentiation and mineralization and were proved to be related to the Erk1/2 pathway which might attribute to the addition of CNTs. It was also reported that MAPK pathways participated in the activation of osteogenic differentiation in *h*BMSCs on random nanofibers mechanotransduction without osteogenic supplement [48]. These results provided useful information for the research and improvement of nanocomposites and also provided dynamic information for the performance of materials in the long-term degradation process.

Overall, CNTs-CaP-CS/Mg composites exhibited good biocompatibility in the long-term degradation process. The addition of Cu might increase the antibacterial properties of the material, making Cu/CNTs-CaP-CS a very promising composites for clinical applications of bone implants, in particular for bone repair and regeneration. So, the following part mainly investigated the Cu/CNTs-CaP-CS/Mg composites.

3.3. Properties of Cu/CNTs-CaP-CS/Mg Composites

3.3.1. The Effect of the Addition of Cu on the Bonding Force and Bioactivity of the CNTs-CaP-CS Coating. Figure 9 displays scratch metallographic photos of CNTs-CaP-CS/Mg with or without the addition of Cu ion. Our previous research showed that CNTs-CaP-CS/Mg possessed satisfactory bonding force [25]. As shown in Figure 9(b), the scratch of Cu/CNTs-CaP-CS/Mg was very smooth and was better than CNTs-CaP-CS/Mg. It could be concluded that the CNTs-CaP-CS coating after Cu deposition will slightly enhance the bonding strength between the coating and the substrate.

Figure 10 shows the release curve of Cu ion after Cu/CNTs-CaP-CS/Mg soaked in m-SBF for 0, 3, 7, 14, 21, and 28 days. As shown in Figure 10, the Cu ion gradually released from the coating before 14 days, peaked at 14 days, and reached a maximum concentration of about 0.025 mg/L.

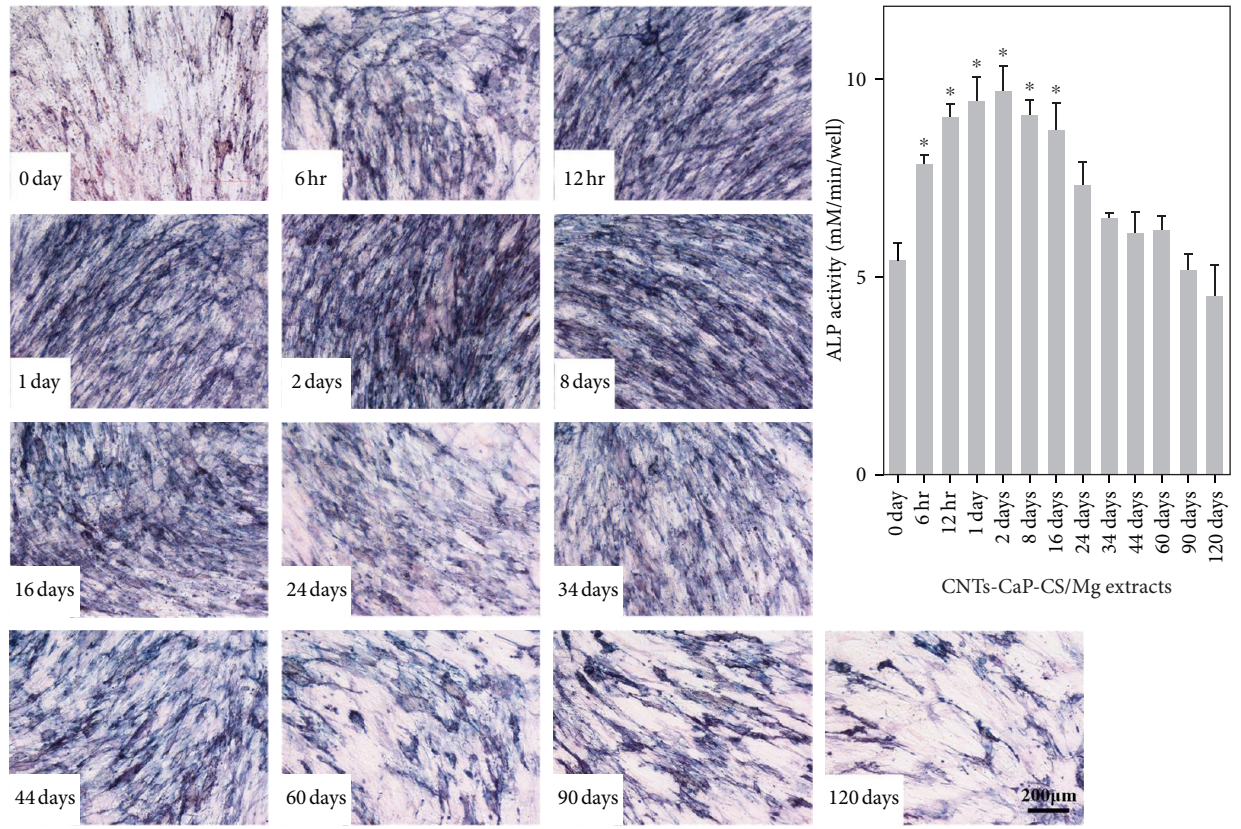

Figure 5: ALP expression stain and quantitative of *h*BMSCs after cultured in different CNTs-CaP-CS/Mg extracts (6, 12 hr, 1, 2, 8, 16, 24, 34, 44, 60, 90, and 120 days). Cells cultured in MSCM containing 50% m-SBF (0 day) were set as the control group ($^{*}P<0.05$).

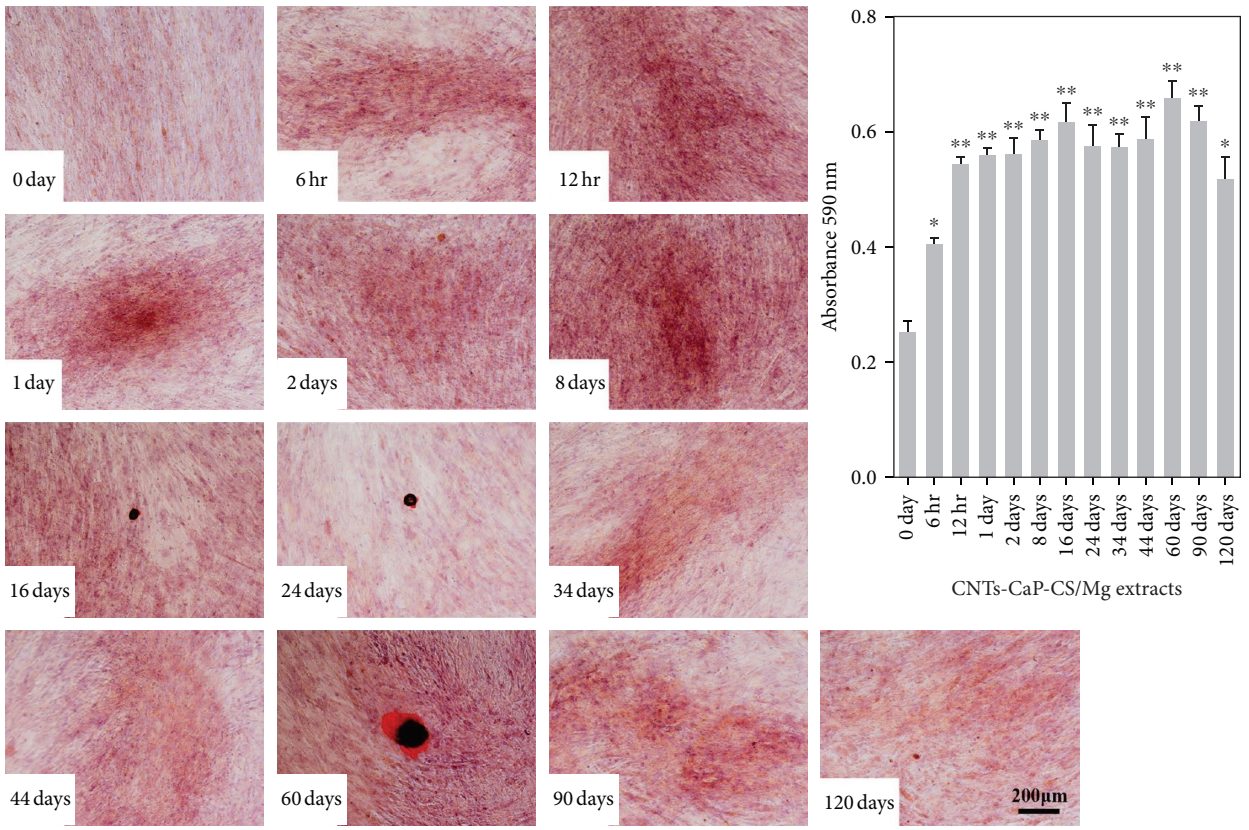

Figure 6: Alizarin Red S stain quantitative of *h*BMSCs after cultured in different CNTs-CaP-CS/Mg extracts (6, 12 hr, 1, 2, 8, 16, 24, 34, 44, 60, 90, and 120 days). Cells cultured in MSCM containing 50% m-SBF (0 day) were set as the control group ($^{*}P<0.05$, $^{**}P<0.01$).

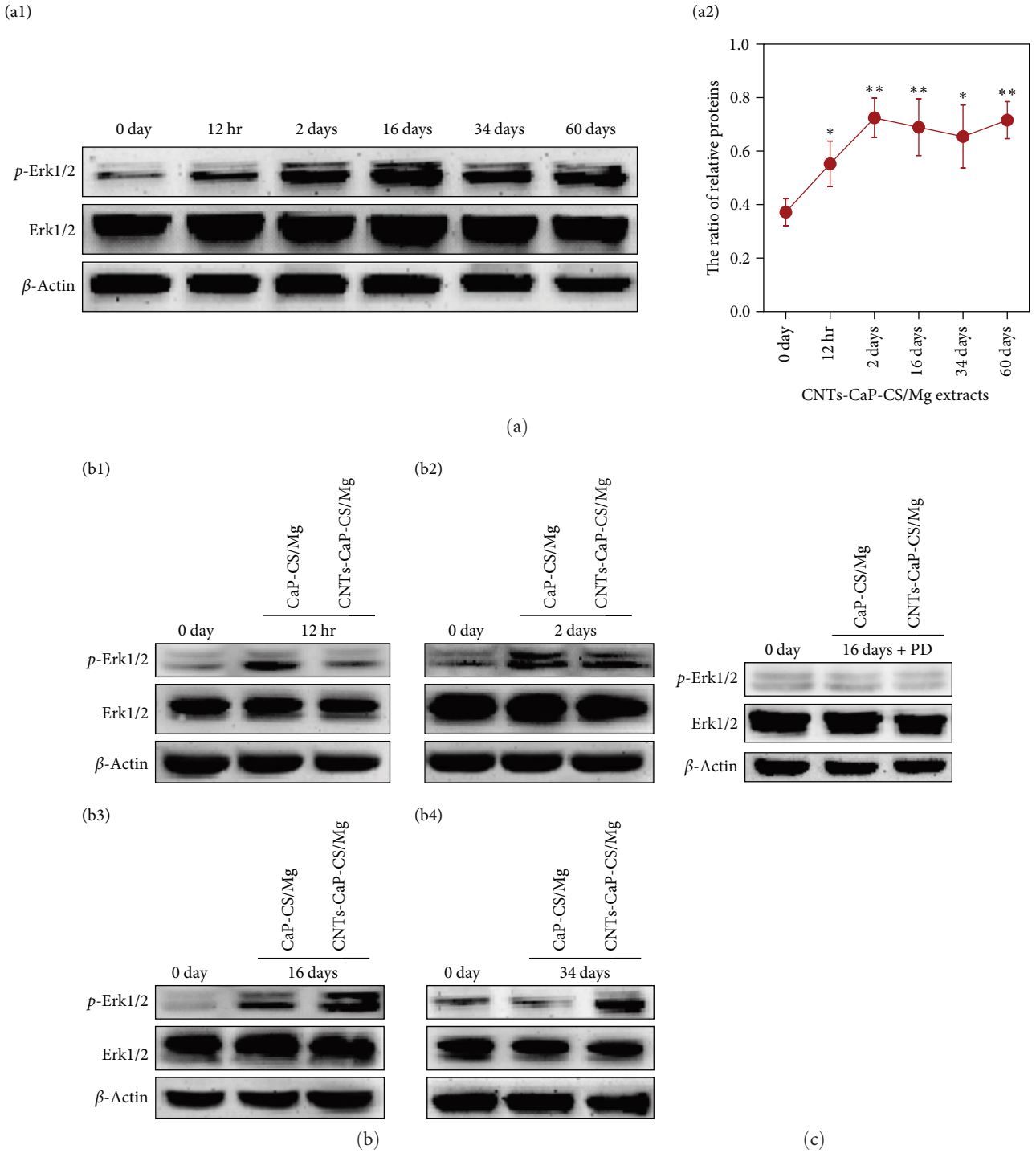

FIGURE 7: Western blot assays were conducted to detect the molecular mechanism of CNTs-CaP-CS/Mg nanocomposites promoting osteogenesis: (a1) immunoblots displaying the p-Erk1/2 in *h*BMSCs after treatment with the CNTs-CaP-CS/Mg extracts (12 hr, 2, 16, 34, and 60 days) for 3 days exposed to the negative control (0 day); (a2) relative expression of p-Erk1/2 to total Erk1/2 protein based on the intensity of bands on the Western blot images. Cells cultured in MSCM containing 50% m-SBF (0 day) were set as the control group ($^{*}P<0.05$, $^{**}P<0.01$); (b) the ratio of protein levels after *h*BMSCs cultured in CNTs-CaP-CS/Mg extracts compared with cultured in CaP-CS/Mg extracts ((b1) 12 hr, (b2) 2 days, (b3) 16 days, (b4) 34 days); (c) immunoblots showing the inhibition effects of Erk1/2-specific inhibitor PD98059 (PD) on the activation of p-Erk1/2 in *h*BMSCs induced by CNTs-CaP-CS/Mg and CaP-CS/Mg 16 days extracts.

After that, the concentration of Cu ions changed little which indicated that the release of Cu ions lasted about 14 days.

Figure 11(a) and 11(b) show that the changing trends of Mg element concentration and pH values of Cu/CNTs-CaP-CS/Mg and CNTs-CaP-CS/Mg in the m-SBF with the immersion time increased from 0 to 28 days, respectively. It could be seen that Mg concentration and pH values increased with the elongation of immersion time which indicated that the CNTs-CaP-CS

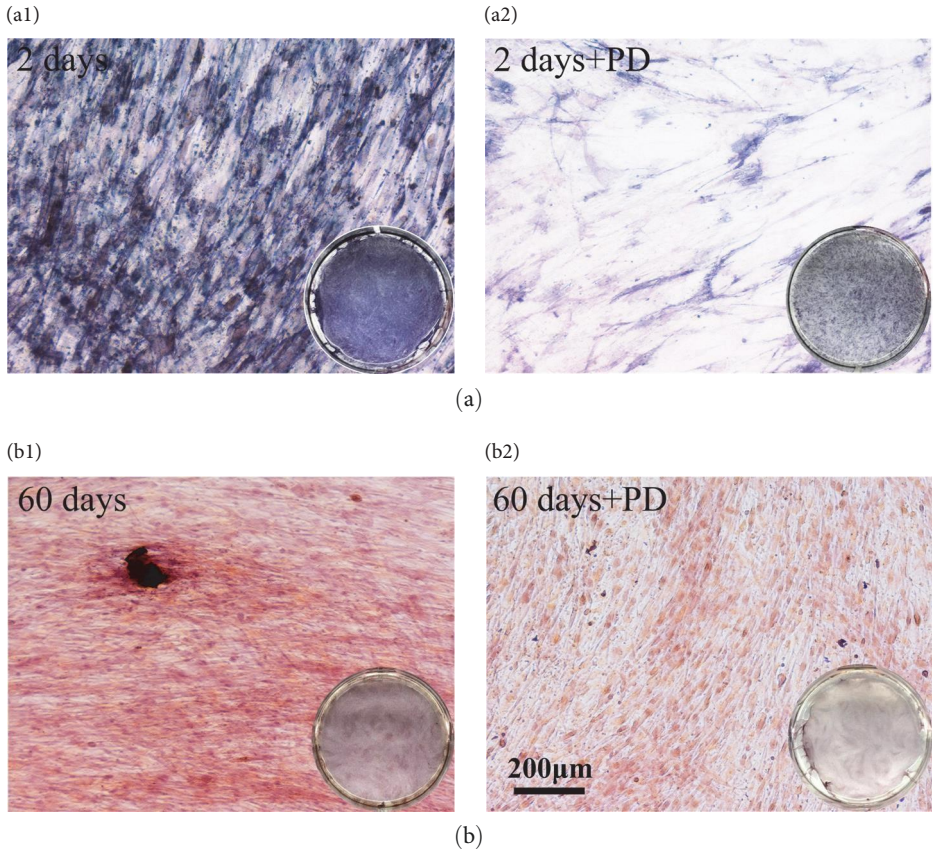

Figure 8: The inhibition of MAPK/Erk on the osteogenic differentiation and mineralization of *h*BMSCs. ALP staining assay after the *h*BMSCs was cultured in CNTs-CaP-CS/Mg 2 days extracts with (a2) or without (a1) 20 mM PD98059 (PD) for 14 days. Alizarin Red S staining assay after the *h*BMSCs was cultured in the CNTs-CaP-CS/Mg 60 days extracts with (b2) or without (b1) 20 mM PD for 14 days.

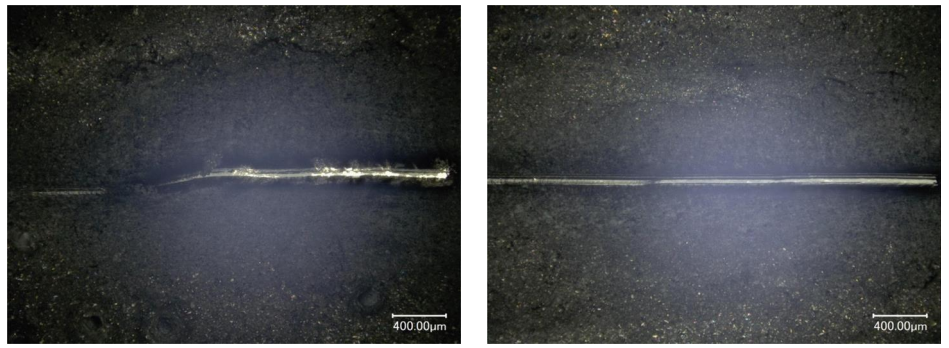

Figure 9: Scratch metallographic photos of (a) CNTs-CaP-CS/Mg (b) and Cu/CNTs-CaP-CS/Mg.

coating with or without Cu element could not totally prevent Mg alloy from the corrosion in m-SBF but slowed down the corrosion rate of magnesium alloy. On the whole, Mg concentration and pH values of Cu/CNTs-CaP-CS/Mg were slightly reduced in comparison with CNTs-CaP-CS/Mg, which indicated that the adhesion between the coating and substrate is slightly enhanced after the inclusion of Cu element and it was consistent with the above scratch experimental results. Figure 11(c) and 11(d) show that Ca and P elements concentrations of Cu/CNTs-CaP-CS/Mg and CNTs-CaP-CS/Mg in the m-SBF with the immersion time increased. It could be clearly seen that Ca and P concentrations in the m-SBF roughly decreased within the whole incubation phase, which indicated that the phosphate grew on the coatings. After the inclusion of the Cu element, the difference in Ca concentration was not obvious and the concentration of P was relatively higher when compared with CNTs-CaP-CS/Mg. The results showed that the bioactivity of the coating was not significantly reduced after the inclusion of the Cu element.

Figure 12(a) shows the XRD pattern of the Cu/CNTs-CaP-CS/Mg that is soaked in the m-SBF for 0, 3, 7, 14, 21, and 28 days. As shown in Figure 12(a), the diffraction peaks of HCA and HA were found in the XRD pattern, indicating that HCA and HA rose on the coating after the Cu/CNTs-CaP-CS/Mg

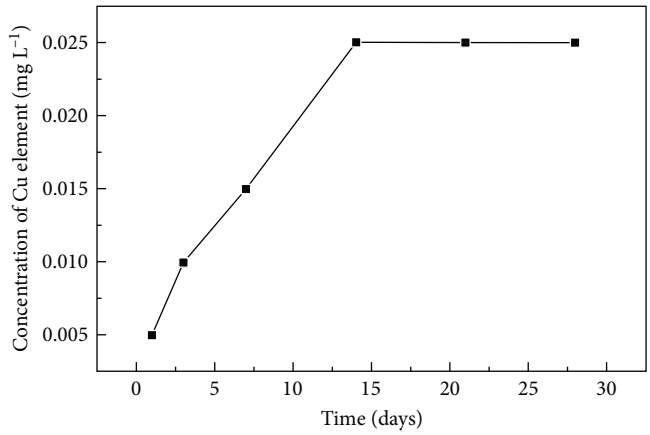

FIGURE 10: The changes of Cu concentration in the extracts of the Cu/CNTs-CaP-CS/Mg with the immersion time increased (1, 3, 7, 14, and 28 days).

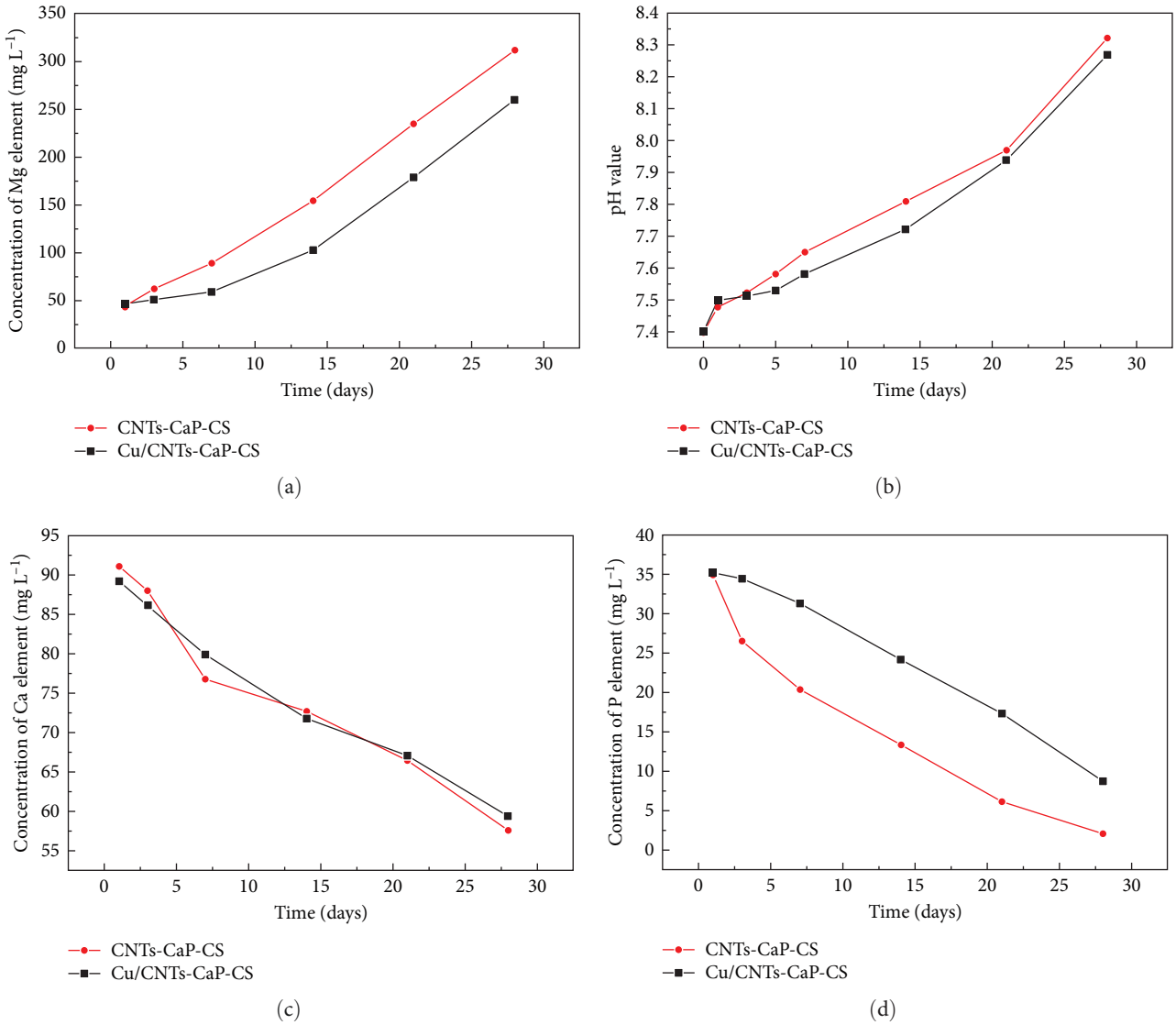

FIGURE 11: The change of different element concentrations and pH values in extracts of CNTs-CaP-CS/Mg and Cu/CNTs-CaP-CS/Mg with the immersion time increased (1, 3, 7, 14, and 28 days): (a) Mg, (b) pH values, (c) Ca, and (d) P.

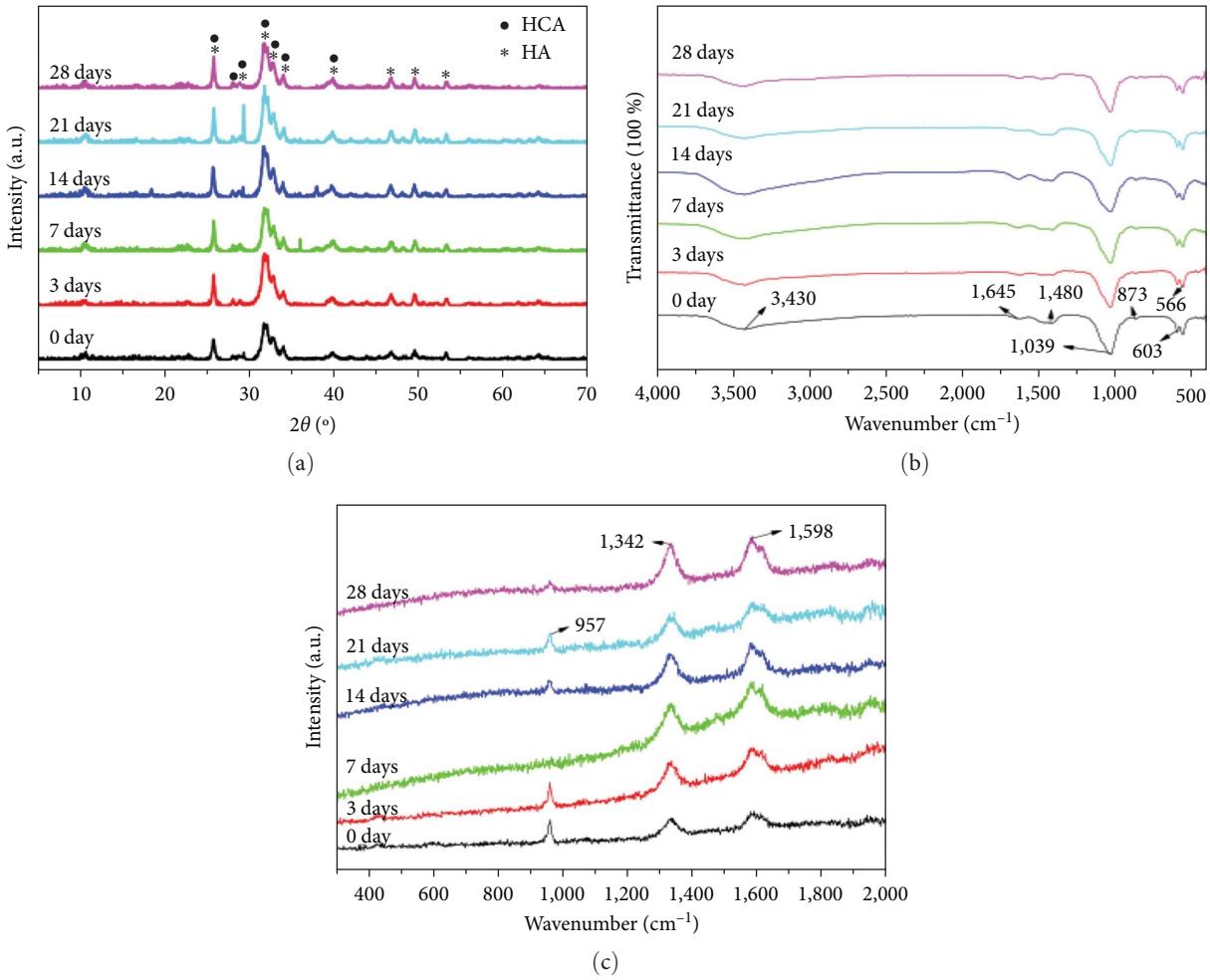

Figure 12: XRD (a), FTIR (b), and Raman spectra (c) of the Cu/CNTs-CaP-CS coating immersed in the m-SBF for different times.

were soaked in m-SBF. While the soaking time transferred from 0 to 28 days the diffraction peaks of HCA and HA became stronger, this indicated that the amount of amorphous HA was increased. Besides, no CNTs peaks are discovered in Figure 12(a), one cause might be that the CNTs were entirely covered by the HA and CS throughout the procedure of EPD and the other cause might be that CNTs' small volume fraction was hard to be observed within XRD's sensitivity limit.

Figure 12(b) shows FTIR spectra of the Cu/CNTs-CaP-CS/Mg after being soaked in the m-SBF for 0, 3, 7, 14, 21, and 28 days. The peaks at 566 and 603 cm^{-1} were attributed to ν_4 P–O bending in the phosphate group. An intense absorption at 1,039 cm^{-1} which refers to ν_3 asymmetrical of P–O that stretched was detected. The bands at 3,430 and 1,645 cm^{-1} were ascribed to stretching and bending vibrations of the hydroxyl (–OH) group. The typical bands at 1,480 (ν_3) and 873 cm^{-1} (ν_2) suggested that the apatite was B-type CO_3^{2-} substitution. With the increase of immersion time, the absorption peaks of 873 cm^{-1} gradually became obvious from 1 to 21 days, which indicated that the amorphous HA on the coating was increased.

Figure 12(c) shows Raman spectra of the Cu/CNTs-CaP-CS/Mg after being soaked in the m-SBF for 0, 3, 7, 14, 21, and 28 days. There were two characteristic peaks at 1,342 and 1,598 cm^{-1} which indicated that CNTs were present in Cu/CNTs-CaP-CS/Mg. The most obvious change was that the characteristic peaks of HA in PO_4^{3-} appeared to be very sharp at 957 cm^{-1} which indicated that the addition of CNTs was favorable for the increment of HA. The 957 cm^{-1} peak was not observed in day 7 extracts, we speculated that the amount of PO_4^{3-} in the extract may be more deposited on the sample surface on the day 7 extracts, so the detected content in the extract is relatively small the 957 cm^{-1} peak not observed. With the extension of the impregnation time, the dissolved amount will increase continuously and the 957 cm^{-1} peak reappeared. Moreover, the peak of 957 cm^{-1} gradually became blunt indicating that the dissolution process of HA is accompanied at the beginning of the growth period. With time increased, the growth of amorphous HA increased. All the XRD, FTIR, and Raman tests showed the Cu/CNTs-CaP-CS/Mg possessed good bioactivity which suggested that the addition of Cu had no reduced influence on the bioactivity of the composites.

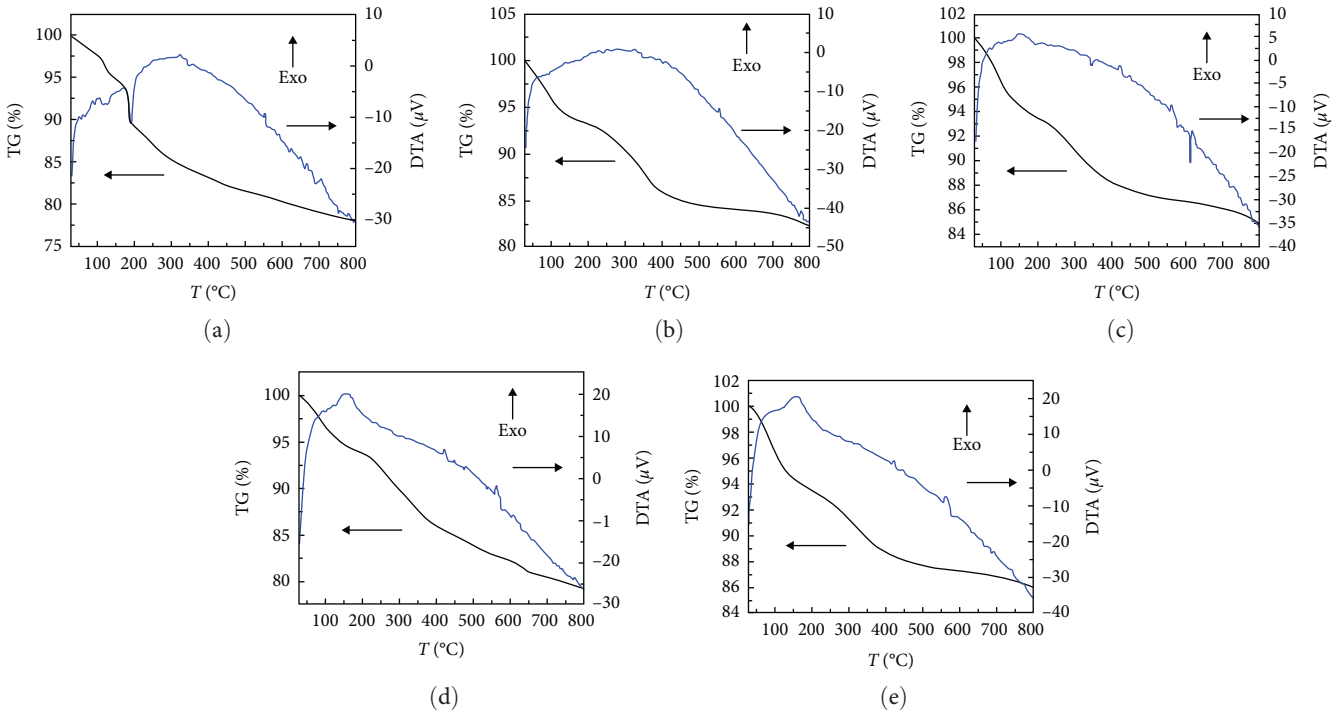

Figure 13: TG and DTA curves of the Cu/CNTs-CaP-CS coating immersed in the m-SBF for different times.: (a) 0 days, (b) 7 days, (c) 14 days, (d) 21 days, and (e) 28 days.

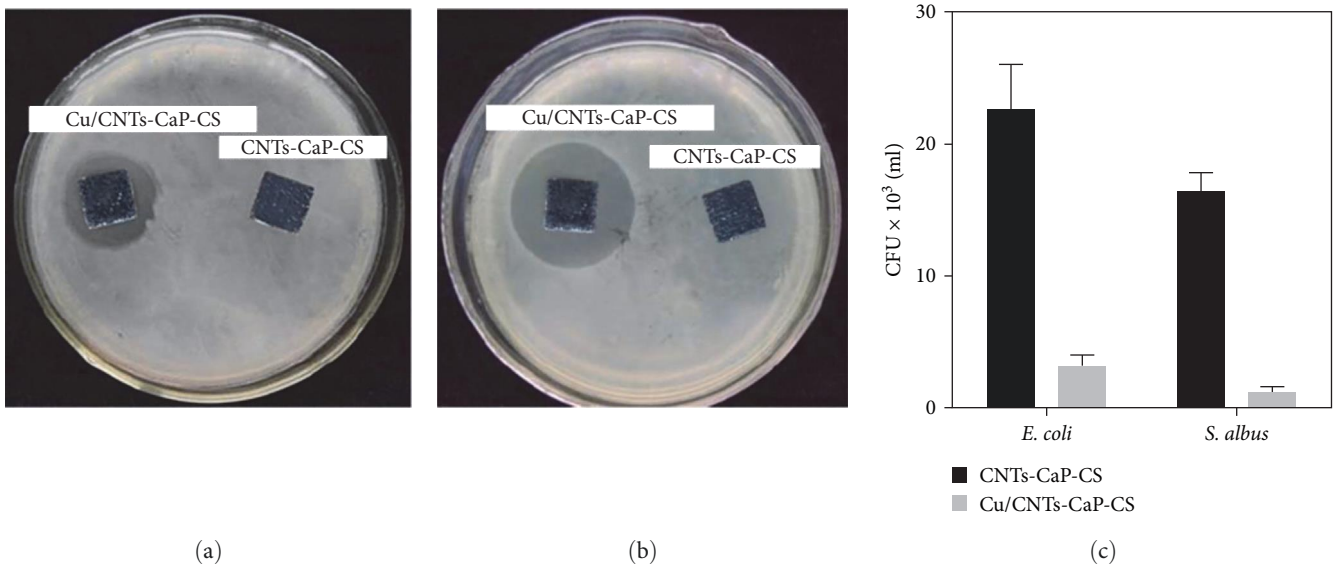

Figure 14: Representative images of agar plates containing CNTs-CaP-CS/Mg and Cu/CNTs-CaP-CS/Mg impregnated film and bacterial inhibition ring for (a) *E. coli* and (b) *S. albus*. Antimicrobial activity of soluble Cu^{2+} against *E. coli* and *S. albus* after 24 hr contact with Cu/CNTs-CaP-CS/Mg (c).

Figure 13 shows that the TG and DTA curves of the Cu/CNTs-CaP-CS/Mg immersed in the m-SBF at different times. The consequences of TG analysis after submersion for 0, 7, 14, 21, and 28 days exhibited a total weight loss of approximate 21.84%, 20.72%, 17.62%, 14.97%, and 13.99% at ~800°C, respectively, which involved the water that was absorbed on the samples and the chitosan in the coating. The composites curves displayed exothermic peaks lower than 500°C, which might be ascribed to the burning out of CS.

3.3.2. Antibacterial Properties of Cu/CNTs-CaP-CS Coating. Figure 14(a) and 14(b) show that the results of the bacterial inhibition ring test and the size of the bacterial inhibition ring around the composite can directly indicate its antibacterial properties. The results showed that the maximum diameter of the bacterial inhibition ring of Cu/CNTs-CaP-CS coating was about 20.6 and 23.4 mm with *E. coli* group and *S. albus* group, respectively, while there was no bacterial inhibition ring when the CNTs-CaP-CS coating in two kinds of bacteria. With immersion time increased, the bacterial

inhibition ring diameter of Cu/CNTs-CaP-CS coating was gradually reduced, *E. coli* group disappeared at 13 days, and *S. albus* group disappeared at 16 days; however, in the two groups, the medium contacted with the coating still had no bacterial growth. The results showed that the Cu/CNTs-CaP-CS coating displayed brilliant antibacterial properties by contrast with CNTs-CaP-CS coating which suggested that Cu on the coating surface plays a key role in killing the bacteria.

Figure 14(c) shows the experimental results of colony-forming units and also *E. coli* and *S. albus* continue to grow after contact with CNTs-CaP-CS coating, while the growth of *E. coli* and *S. albus* on the culture medium was significantly reduced after contact with Cu/CNTs-CaP-CS coating. The antibacterial rate of Cu/CNTs-CaP-CS coating against *E. coli* was 85.84% and the *S. albus* was 92.27%.

At pHs below the pKa, most amino groups are protonated and turn into a cationic polyelectrolyte (Equation (1)). When *n*HA, CS, CNTs and $Cu(NO_3)_2$ (or without) particles sequentially added into the acetic acid aqueous solution, *n*HA were dissolved and then Ca^{2+} ions would be released (Equation (2)) [25]:

$$\text{CHIT} - \text{NH}_2 + \text{H}_3\text{O}^+ \longrightarrow \text{CHIT} - \text{NH}_3^+ + \text{H}_2\text{O}, \quad (1)$$

$$\text{Ca}_{10}(\text{PO}_4)_6(\text{OH})_2 + 2\text{H}^+ \longrightarrow 10\text{Ca}^{2+} + 6\text{PO}_4^{3-} + 2\text{H}_2\text{O}. \quad (2)$$

The above cations like Cu^{2+}, Ca^{2+}, and H^+ as well as $\text{CHIT} - \text{NH}_3^+$ adsorbed on the *n*HA and CNTs surfaces provided the electrostatic stabilization and charging of the *n*HA (Equation (3)) and CNTs particles (Equation (4)).

$$\text{CNTs} + \text{CHIT} - \text{NH}_3^+ \longrightarrow \text{CNTs} - \text{CHIT} - \text{NH}_3^+, \quad (3)$$

$$n\text{HA} + \text{CHIT} - \text{NH}_3^+ \longrightarrow n\text{HA} - \text{CHIT} - \text{NH}_3^+. \quad (4)$$

The performances of the particle dispersion, high suspension stability, as well as, the sediment layers, and the EPD process are affected through the suspension performances, like stability, conductivity, transmittance particle size, and ζ-potential, as well as the quantity of dispersants [49]. The movement speed of *n*HA and CNTs particles depended on the Smoluchowski equation [50], with the addition of CS-acetic acid aqueous solution, the ionic conductivity and ζ-potential grew. The local higher ζ-potential would advance the charging *n*HA and CNTs particles transferred speedily and the large quantity of free ions like Cu^{2+}, Ca^{2+}, and H^+ might become principal current carriers and hence the addition of Cu^{2+} might increase the particles moved rapidly. With the extension of current loading time, more and more H_2 released, and rapid diffusion of OH^- in the electrolyte would cause the pH change around the metal/solution interface (Equation (5)).

$$2\text{H}_2\text{O} + 2\text{e}^- \longrightarrow \text{H}_2\uparrow + 2\text{OH}^-. \quad (5)$$

As pH is higher than 6.5, amino groups in CS tended to be deprotonated (Equation (6)) and then deposited on the cathode's surface, which was accompanied by insoluble Ca $(OH)_2$ layers (Equation (7)) and the complexation reaction between CS and Cu^{2+} (Equation (8)), as well as the heterocoagulation of *n*HA and CNTs. With deposit time increase, more and more $Ca(OH)_2$ deposited in the layers, which would advance the formation of CS, complexation reaction between CS and Cu^{2+}, and *n*HA particles and CNTs was tightly entrapped into CS and Cu complexation layers.

$$\text{CHIT} - \text{NH}_3^+ + \text{OH}^- \longrightarrow \text{CHIT} - \text{NH}_2 + \text{H}_2\text{O}, \quad (6)$$

$$\text{Ca}^{2+} + 2\text{OH}^- \longrightarrow \text{Ca}(\text{OH})_2\downarrow, \quad (7)$$

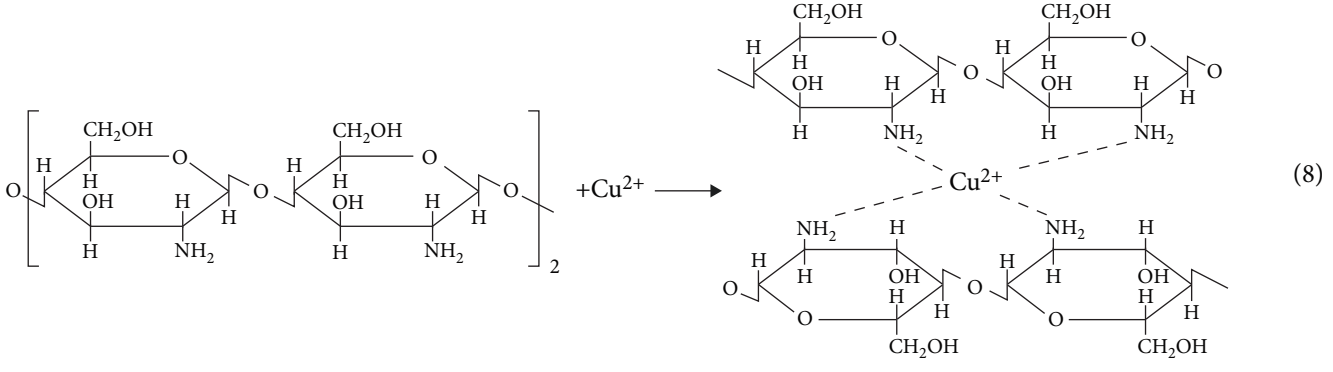

(8)

The experimental results indicated that both *E. coli* and *S. albus* activities were suppressed after contact with the Cu/CNTs-CaP-CS coating, in which released Cu ion in the bacterial solution plays a key role. Research has shown that Cu nanoparticles–organism interface showed a significant interaction and the bactericidal mechanism may be related to contact killing [36]. Cu exhibits excellent antibacterial properties and its released amount is very little, it makes

such substances extremely safe as one kind of long-lasting biocide [51]. The antibacterial property of Cu was ascribed chiefly to adhesion with bacteria which led to the reduction reaction on the cell wall of bacteria due to their opposite electrical charges [35]. The bactericidal mechanism of Cu/CNTs-CaP-CS/Mg coating might be related to the release and contact killing of Cu ions into the bacterial solution. The molecular structure of CS contains hydroxyl, amino, and other active groups, which have strong coordination ability with metal ions. In the crosslinking reaction of CS with Cu, the hydroxyl and amino groups of chitosan take part in the reaction, especially for the amino reaction. In addition, the formation of physical network by complexation reaction between CS and Cu^{2+} and *n*HA particles might promote antibacterial properties of materials. The Cu/CNTs-CaP-CS coating showed excellent antibacterial properties which might be due to the physical network. It suggests that the Cu/CNTs-CaP-CS/Mg composites can be considered potential bone implants as a biocide in the field of medicine. Overall, CNTs-CaP-CS/Mg composites exhibited good biocompatibility in the long-term degradation process which possessed the potential to become a bone implant material. The addition of Cu increased the antibacterial properties of the material, making Cu/CNTs-CaP-CS a very promising composites for clinical applications of bone implants, in particular for bone repair and regeneration. Further work is needed to investigate the specific experiment, mechanism, and biocompatibility of the Cu/CNTs-CaP-CS/Mg composites.

4. Conclusion

In this paper, the CNTs-CaP-CS/Mg extracts, especially the 24 days extract was suitable for SaOS-2 cells proliferation and differentiation when the immersion time changed from 6 hr to 90 days which indicated that the degradation product of the composites would not result in cell toxicity. Stimulated by the CNTs-CaP-CS/Mg extracts, the ALP expression of *h*BMSCs increased in the first 16 days and the mineralization ability of *h*BMSCs is highly kept throughout the whole process through the Erk1/2 signaling pathway. After the CNTs-loaded Cu element, the bonding strength between the substrate and the coating was slightly enhanced and the bioactivity of the coating was satisfactory. The studies of antimicrobial activity showed that Cu/CNTs-CaP-CS/Mg had efficient antibacterial activity against *E. coli* and *S. albus*. For this reason, the Cu/CNTs-CaP-CS/Mg can be applied as a bactericidal coating, whose antibacterial effect might be due to the formation of the physical network by complexation reaction between CS and Cu^{2+} and *n*HA particles. CNTs-CaP-CS/Mg composites exhibited good biocompatibility in the long-term degradation process. The addition of Cu increased the antibacterial properties of the material, making Cu/CNTs-CaP-CS a very promising composites for clinical applications of bone implants.

Abbreviations

Mg: Magnesium
CS: Chitosan
CNTs: Carbon nanotubes
Cu: Copper
SaOS-2: Human osteosarcoma cell line
*h*BMSCs: Human bone marrow mesenchymal stem cells
MAO: Microarc oxidized
*n*HA: Nanohydroxyapatite
EPD: Electrophoresis deposition
DAPI: 4′,6-diamidino-2-phenylindole
FITC: Fluorescein isothiocyanate
PI: Propidium iodide
ALP: Alkaline phosphatase
PNP: p-nitrophenol
PMSF: Phenylmethylsulphonyl fluoride
PVDF: Polyvinylidene fluoride
XRD: X-ray diffractometer
FTIR: Fourier-transformed infrared spectrophotometer
TG: Thermogravimetric
DTA: Differential thermal analyzer
E. coli: *Escherichia coli*
S. albus: *Staphylococcus albus*.

Data Availability

The raw data used to support the findings of this study are available from the corresponding author upon request.

Conflicts of Interest

The authors declare that they have no conflicts of interest.

Authors' Contributions

Conceptualization, Z.W., C.D. and R.S.; methodology, Z.W. and M.Z.; software, M.Z. and L.J.; validation, Z.W., C.D. and R.S.; formal analysis, Z.W.; investigation, M.Z. and L.J.; resources, Z.W., C.D. and R.S.; data curation, M.Z., L.J., Y.Z. and H.W.; writing—original draft preparation, M.Z.; writing—review and editing, Z.W.; visualization, M.Z.; supervision, Z.W. and C.D.; project administration, Z.W.; funding acquisition, Z.W. All authors have read and agreed to the published version of the manuscript.

Funding

This work was funded by the National Natural Science Foundation of China (Nos. 51873052 and 51272058).

References

[1] L. Tan, X. Yu, P. Wan, and K. Yang, "Biodegradable materials for bone repairs: a review," *Journal of Materials Science & Technology*, vol. 29, no. 6, pp. 503–513, 2013.

[2] X.-N. Gu and Y.-F. Zheng, "A review on magnesium alloys as biodegradable materials," *Frontiers of Materials Science in China*, vol. 4, pp. 111–115, 2010.

[3] D. Persaud-Sharma and A. McGoron, "Biodegradable magnesium alloys: a review of material development and applications," *Journal of Biomimetics, Biomaterials and Tissue Engineering*, vol. 12, pp. 25–39, 2012.

[4] G. E. J. Poinern, S. Brundavanam, and D. Fawcett, "Biomedical magnesium alloys: a review of material properties, surface

modifications and potential as a biodegradable orthopaedic implant," *American Journal of Biomedical Engineering*, vol. 2, no. 6, pp. 218–240, 2012.

[5] S. Jafari, S. E. Harandi, and R. K. Singh Raman, "A review of stress-corrosion cracking and corrosion fatigue of magnesium alloys for biodegradable implant applications," *JOM*, vol. 67, pp. 1143–1153, 2015.

[6] H. S. Brar, M. O. Platt, M. Sarntinoranont, P. I. Martin, and M. V. Manuel, "Magnesium as a biodegradable and bioabsorbable material for medical implants," *JOM*, vol. 61, pp. 31–34, 2009.

[7] M. P. Staiger, A. M. Pietak, J. Huadmai, and G. Dias, "Magnesium and its alloys as orthopedic biomaterials: a review," *Biomaterials*, vol. 27, no. 9, pp. 1728–1734, 2006.

[8] N.-E. L. Saris, E. Mervaala, H. Karppanen, J. A. Khawaja, and A. Lewenstam, "Magnesium: an update on physiological, clinical and analytical aspects," *Clinica Chimica Acta*, vol. 294, no. 1-2, pp. 1–26, 2000.

[9] S. Nayak, B. Bhushan, R. Jayaganthan, P. Gopinath, R. D. Agarwal, and D. Lahiri, "Strengthening of Mg based alloy through grain refinement for orthopaedic application," *Journal of the Mechanical Behavior of Biomedical Materials*, vol. 59, pp. 57–70, 2016.

[10] L. Xu, E. Zhang, D. Yin, S. Zeng, and K. Yang, "In vitro corrosion behaviour of Mg alloys in a phosphate buffered solution for bone implant application," *Journal of Materials Science: Materials in Medicine*, vol. 19, pp. 1017–1025, 2008.

[11] F. Witte, "The history of biodegradable magnesium implants: a review," *Acta Biomaterialia*, vol. 6, no. 5, pp. 1680–1692, 2010.

[12] T. S. N. Sankara Narayanan, I. S. Park, and M. H. Lee, "Strategies to improve the corrosion resistance of microarc oxidation (MAO) coated magnesium alloys for degradable implants: prospects and challenges," *Progress in Materials Science*, vol. 60, no. 3, pp. 1–71, 2014.

[13] N. Shadjou and M. Hasanzadeh, "Graphene and its nanostructure derivatives for use in bone tissue engineering: recent advances," *Journal of Biomedical Materials Research Part A*, vol. 104, no. 5, pp. 1250–1275, 2016.

[14] L.-G. Yu, K. A. Khor, H. Li, and P. Cheang, "Effect of spark plasma sintering on the microstructure and in vitro behavior of plasma sprayed HA coatings," *Biomaterials*, vol. 24, no. 16, pp. 2695–2705, 2003.

[15] C. Shuai, Y. Zhou, Y. Yang et al., "Biodegradation resistance and bioactivity of hydroxyapatite enhanced Mg–Zn composites via selective laser melting," *Materials*, vol. 10, no. 3, Article ID 307, 2017.

[16] Z. Fan, J. Wang, Z. Wang et al., "One-pot synthesis of graphene/hydroxyapatite nanorod composite for tissue engineering," *Carbon*, vol. 66, pp. 407–416, 2014.

[17] J.-K. Francis Suh and H. W. T. Matthew, "Application of chitosan-based polysaccharide biomaterials in cartilage tissue engineering: a review," *Biomaterials*, vol. 21, no. 24, pp. 2589–2598, 2000.

[18] N. Mighri, J. Mao, F. Mighri, A. Ajji, and M. Rouabhia, "Chitosan-coated collagen membranes promote chondrocyte adhesion, growth, and interleukin-6 secretion," *Materials*, vol. 8, no. 11, pp. 7673–7689, 2015.

[19] S. Kalmodia, S. Goenka, T. Laha, D. Lahiri, B. Basu, and K. Balani, "Microstructure, mechanical properties, and *in vitro* biocompatibility of spark plasma sintered hydroxyapatite–aluminum oxide–carbon nanotube composite," *Materials Science and Engineering: C*, vol. 30, no. 8, pp. 1162–1169, 2010.

[20] K. Balani, R. Anderson, T. Laha et al., "Plasma-sprayed carbon nanotube reinforced hydroxyapatite coatings and their interaction with human osteoblasts in vitro," *Biomaterials*, vol. 28, no. 4, pp. 618–624, 2007.

[21] X. Li, X. Liu, J. Huang, Y. Fan, and F.-Z. Cui, "Biomedical investigation of CNT based coatings," *Surface and Coatings Technology*, vol. 206, no. 4, pp. 759–766, 2011.

[22] T. Akasaka, A. Yokoyama, M. Matsuoka et al., "Adhesion of human osteoblast-like cells (Saos-2) to carbon nanotube sheets," *Bio-Medical Materials and Engineering*, vol. 19, no. 2-3, pp. 147–153, 2009.

[23] T. Akasaka, A. Yokoyama, M. Matsuoka, T. Hashimoto, and F. Watari, "Thin films of single-walled carbon nanotubes promote human osteoblastic cells (Saos-2) proliferation in low serum concentrations," *Materials Science and Engineering: C*, vol. 30, no. 3, pp. 391–399, 2010.

[24] X. Li, H. Liu, X. Niu et al., "The use of carbon nanotubes to induce osteogenic differentiation of human adipose-derived MSCs *in vitro* and ectopic bone formation *in vivo*," *Biomaterials*, vol. 33, no. 19, pp. 4818–4827, 2012.

[25] J. Zhang, Z. Wen, M. Zhao, G. Li, and C. Dai, "Effect of the addition CNTs on performance of CaP/chitosan/coating deposited on magnesium alloy by electrophoretic deposition," *Materials Science and Engineering: C*, vol. 58, pp. 992–1000, 2016.

[26] L. F. Zemljič, Z. Peršin, and P. Stenius, "Improvement of chitosan adsorption onto cellulosic fabrics by plasma treatment," *Biomacromolecules*, vol. 10, no. 5, pp. 1181–1187, 2009.

[27] C.-M. Shih, Y.-T. Shieh, and Y.-K. Twu, "Preparation and characterization of cellulose/chitosan blend films," *Carbohydrate Polymers*, vol. 78, no. 1, pp. 169–174, 2009.

[28] Z. Deng, H. Zhu, B. Peng et al., "Synthesis of PS/Ag nanocomposite spheres with catalytic and antibacterial activities," *ACS Applied Materials & Interfaces*, vol. 4, no. 10, pp. 5625–5632, 2012.

[29] X. Yao, X. Zhang, H. Wu, L. Tian, Y. Ma, and B. Tang, "Microstructure and antibacterial properties of Cu-doped TiO_2 coating on titanium by micro-arc oxidation," *Applied Surface Science*, vol. 292, pp. 944–947, 2014.

[30] H. H. A. Dollwet and J. R. J. Sorenson, "Historic uses of copper compounds in medicine," *Trace Elements in Medicine*, vol. 2, pp. 80–87, 1985.

[31] H. Chai, L. Guo, X. Wang et al., "Antibacterial effect of 317L stainless steel contained copper in prevention of implant-related infection in vitro and in vivo," *Journal of Materials Science: Materials in Medicine*, vol. 22, pp. 2525–2535, 2011.

[32] A. Simchi, E. Tamjid, F. Pishbin, and A. R. Boccaccini, "Recent progress in inorganic and composite coatings with bactericidal capability for orthopaedic applications," *Nanomedicine: Nanotechnology, Biology and Medicine*, vol. 7, no. 1, pp. 22–39, 2011.

[33] L. Weaver, H. T. Michels, and C. W. Keevil, "Survival of *Clostridium difficile* on copper and steel: futuristic options for hospital hygiene," *The Journal of Hospital Infection*, vol. 68, no. 2, pp. 145–151, 2008.

[34] C. Wu, Y. Zhou, M. Xu et al., "Copper-containing mesoporous bioactive glass scaffolds with multifunctional properties of angiogenesis capacity, osteostimulation and antibacterial activity," *Biomaterials*, vol. 34, no. 2, pp. 422–433, 2013.

[35] M. Raffi, S. Mehrwan, T. M. Bhatti et al., "Investigations into the antibacterial behavior of copper nanoparticles against *Escherichia coli*," *Annals of Microbiology*, vol. 60, pp. 75–80, 2010.

[36] N. C. Cady, J. L. Behnke, and A. D. Strickland, "Copper-based nanostructured coatings on natural cellulose: nanocomposites

exhibiting rapid and efficient inhibition of a multi-drug resistant wound pathogen, *A. baumannii*, and mammalian cell biocompatibility in vitro," *Advanced Functional Materials*, vol. 21, no. 13, pp. 2506–2514, 2011.

[37] C. Wu, Z. Wen, C. Dai, Y. Lu, and F. Yang, "Fabrication of calcium phosphate/chitosan coatings on AZ91D magnesium alloy with a novel method," *Surface and Coatings Technology*, vol. 204, no. 20, pp. 3336–3347, 2010.

[38] J. Zhang, C. Dai, J. Wei, Z. Wen, S. Zhang, and C. Chen, "Degradable behavior and bioactivity of micro-arc oxidized AZ91D Mg alloy with calcium phosphate/chitosan composite coating in m-SBF," *Colloids and Surfaces B: Biointerfaces*, vol. 111, pp. 179–187, 2013.

[39] T. Kokubo and H. Takadama, "How useful is SBF in predicting in vivo bone bioactivity?" *Biomaterials*, vol. 27, no. 15, pp. 2907–2915, 2006.

[40] M. Zhao, Y. Dai, X. Li et al., "Evaluation of long-term biocompatibility and osteogenic differentiation of graphene nanosheet doped calcium phosphate-chitosan AZ91D composites," *Materials Science and Engineering: C*, vol. 90, pp. 365–378, 2018.

[41] H. M. Wong, K. W. K. Yeung, K. O. Lam et al., "A biodegradable polymer-based coating to control the performance of magnesium alloy orthopaedic implants," *Biomaterials*, vol. 31, no. 8, pp. 2084–2096, 2010.

[42] Z. Wang, J. Yan, J. Li et al., "Effects of biodegradable Mg–6Zn alloy extracts on apoptosis of intestinal epithelial cells," *Materials Science and Engineering: B*, vol. 177, no. 4, pp. 388–393, 2012.

[43] Y.-L. Chang, C. M. Stanford, and J. C. Keller, "Calcium and phosphate supplementation promotes bone cell mineralization: implications for hydroxyapatite (HA)-enhanced bone formation," *Journal of Biomedical Materials Research*, vol. 52, no. 2, pp. 270–278, 2000.

[44] S. Maeno, Y. Niki, H. Matsumoto et al., "The effect of calcium ion concentration on osteoblast viability, proliferation and differentiation in monolayer and 3D culture," *Biomaterials*, vol. 26, no. 23, pp. 4847–4855, 2005.

[45] R. Tatavarty, H. Ding, G. Lu, R. J. Taylor, and X. Bi, "Synergistic acceleration in the osteogenesis of human mesenchymal stem cells by graphene oxide–calcium phosphate nanocomposites," *Chemical Communications*, vol. 50, no. 62, pp. 8484–8487, 2014.

[46] F. Yang, D. Yang, J. Tu, Q. Zheng, L. Cai, and L. Wang, "Strontium enhances osteogenic differentiation of mesenchymal stem cells and in vivo bone formation by activating Wnt/catenin signaling," *Stem Cells*, vol. 29, no. 6, pp. 981–991, 2011.

[47] S. Duan, X. Yang, F. Mei et al., "Enhanced osteogenic differentiation of mesenchymal stem cells on poly(L-lactide) nanofibrous scaffolds containing carbon nanomaterials," *Journal of Biomedical Materials Research Part A*, vol. 103, no. 4, pp. 1424–1435, 2015.

[48] W. Liu, Y. Wei, X. Zhang, M. Xu, X. Yang, and X. Deng, "Lower extent but similar rhythm of osteogenic behavior in hBMSCs cultured on nanofibrous scaffolds *versus* induced with osteogenic supplement," *ACS Nano*, vol. 7, no. 8, pp. 6928–6938, 2013.

[49] J. Chen, J. Wang, E. Han, J. Dong, and W. Ke, "AC impedance spectroscopy study of the corrosion behavior of an AZ91 magnesium alloy in 0.1 M sodium sulfate solution," *Electrochimica Acta*, vol. 52, no. 9, pp. 3299–3309, 2007.

[50] J. Zhang, C. Dai, Z. Wen, and J. Wei, "Study on the effect of the coating thickness on corrosion behavior of AZ91D magnesium alloy in m-SBF," *International Journal of Electrochemical Science*, vol. 10, pp. 6002–6013, 2015.

[51] J. Drelich, B. Li, P. Bowen, J.-Y. Hwang, O. Mills, and D. Hoffman, "Vermiculite decorated with copper nanoparticles: novel antibacterial hybrid material," *Applied Surface Science*, vol. 257, no. 22, pp. 9435–9443, 2011.